VISUAL EXPERIMENTAL STUDY ON START-UP AND HEAT TRANSFER CHARACTERISTICS OF FLAT-PLATE PULSATING HEAT PIPE

Xin CAO[1], Fumin SHANG[1, 2,*], Chaofan ZHENG[1], Kai YANG[1], Haoran XU[1], Shunfang MA[1], Jianhong LIU[1], Dong LIU[1]

[1] Changchun Institute of Technology, School of Energy and Power Engineering, China Changchun, China

[2] Jilin School-Enterprise Joint Innovation Laboratory of Thermal Management Technology, China Changchun, China

* Corresponding author; E-Mail: fuminshang@ccit.edu.cn

The flat-plate pulsating heat pipe (FP-PHP) offers several advantages, including a simple structure, low cost, high reliability, and effective heat transfer performance. These attributes contribute to its widespread use in the heat dissipation of various electronic devices. The operation of a FP-PHP involves a complex process of phase change heat transfer. To gain a clearer understanding of how the working fluid behaves within the FP-PHP, this paper presents a visualization experiment focused on FP-PHP with rectangular cross-section channels. The experiment primarily examines the start-up and heat transfer characteristics of the FP-PHP under different heating powers and inclination angles. Additionally, it analyzes the vapor-liquid two-phase flow patterns within the pipe under various operating conditions. Experimental results indicate that as heating power increases, the flow pattern in the evaporation section of the FP-PHP changes from a plug-shaped flow to a local annular flow, and subsequently from a local annular flow to a global annular flow. Higher heating power results in a shorter start-up time and a higher start-up temperature for the FP-PHP. The heat transfer characteristics are optimal when the inclination angle is at 90°. At this angle, with a heating power of 120 W, the thermal resistance of the FP-PHP measures only 0.51 ℃/W.

Key words*: flat-plate pulsating heat pipe, flow visualization, nucleation start-up, heating power*

1. Introduction

Pulsating heat pipe has the advantages of simple structure, low cost, high reliability, and good heat transfer performance, which makes it show good application prospects in the fields of microelectronics cooling, waste heat recovery, solar thermal collector and refrigeration and air conditioning [1–3].

Pulsating heat pipes represent a new type of high-efficiency heat transfer element that involves a complex phase change heat transfer process. Many researchers have conducted experimental studies to investigate various factors that affect the heat transfer performance of pulsating heat pipes. These

factors include the working material [4], liquid filling rate [5], cross-sectional shape [6], inclination angle [7], and heating power [8]. In addition to this, the start-up characteristics of the pulsating heat pipe are a key factor in expanding its place of use. Pulsating heat pipe startup is a dynamic process where heat is applied to the evaporator until the unit reaches a quasi-steady state, delivering heat to the condenser without overheating [9]. Two sets of trapezoidal cross-section silicon-based micropulse heat pipes (SMPHPs) with hydraulic diameters of 352 μm (#1) and 394 μm (#2) were fabricated for the first time by Qu et al. [2] using MEMS technology. It was found that no nucleation was observed during the startup phase, and vapor plugs at the evaporator U-bend were formed mainly due to the rupture of the liquid phase. Nucleation boiling occurred only in SMPHP (#2) at relatively high power inputs. Tong et al. [10] visualized a closed-loop pulsating heat pipe (PHP) flow using a charge-coupled device (CCD). The results suggest that meandering bends, uneven slug and clog distributions, and non-parallel boiling at the evaporator are the driving and restoring forces responsible for the circulation and oscillation of the fluid. Liu et al. [11] introduced control theory (system identification theory) to quantitatively analyze the startup performance of closed-loop pulsating heat pipes (CLPHPs) based on experimental studies of various working fluids under different operating conditions. The analysis shows that the start-up performance of CLPHPs increases with increasing inclination angle from 0° to 90°. With the increase in thermal load, the startup speed increases and the relative stability increases while the startup temperature increases.

This article presents a visual experimental study on FP-PHP with rectangular cross-sectional channels. The study analyzes the start-up and heat transfer performance of the heat pipe under varying heating powers and inclination angles. This analysis includes examining the wall temperature of the FP-PHP, the changes in the flow pattern of the working fluid inside the pipe, and the variations in pressure within the system. The findings of this research aim to provide a valuable reference for the application of FP-PHPs designed and developed according to hydrodynamic characteristics.

2. Research Method

2.1. Experimental Setup
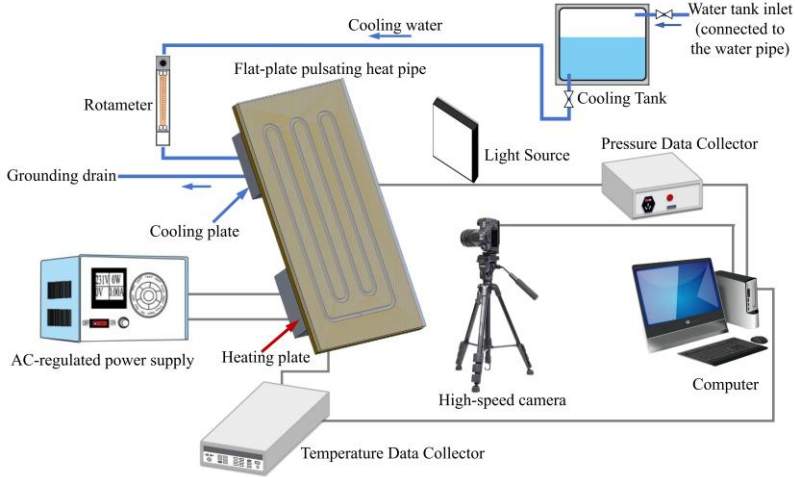
Fig.1 Schematic diagram of FP-PHP experimental system

Fig. 1 shows the schematic diagram of the FP-PHP visualization experiment system. The experimental system mainly includes the FP-PHP experimental body, heating system, cooling system, and data acquisition system. The FP-PHP experimental body consists of a copper plate milled with serpentine curved rectangular channels, a transparent acrylic plate, a heating plate, a cooling plate, and a stainless steel support frame, as shown in Fig. 2. The 3M VHB clear double-sided adhesive provides continuous high-temperature resistance up to 120 ℃ and is used to bond the copper plate to the transparent acrylic plate. The copper plate, clear acrylic, and 3M VHB double-sided adhesive were securely fastened with bolts to ensure a tight seal of the channel. The backside of the copper plate was coated with thermally conductive silicone grease (model QM850, thermal conductivity 4.15 W/(m·K)) to minimize contact thermal resistance with both the heating plate and the cooling plate. The FP-PHP, heating plate, and cooling plate are arranged on stainless steel support frame, with insulating cotton used to prevent additional heat loss. The stainless steel support frame is mounted on a rotatable platform. In this experiment, the power output of the heating plate is controlled by the AC regulated power supply, which has a power adjustment range of 0 to 500 W. The dimensions of the heating plate are 100 mm × 50 mm × 20 mm (length × width × height), and it can withstand a maximum power of 300 W and a maximum working temperature of 350 ℃. The cooling plate measures 100 mm × 40 mm × 12 mm (length × width × height), with its inlet and outlet water pipes located on the same side of the plate. The water pipe near the adiabatic section serves as the inlet pipe. The model of the rotameter used is LZB-10, which has a measurement range of 10 to 100 L/h and an accuracy of ± 2.5%. For this experiment, the cooling water flow rate is set to a constant value of 60 L/h. The data acquisition system comprises a high-speed camera, an Agilent 34972A data collector, a high-precision K-type thermocouple, a pressure data collector, a pressure sensor, and a computer. The temperature measurement range of the type K thermocouple is from 0 to 1300 ℃, with a measurement error of ± 0.1 ℃. A high-speed video camera and a cell phone were utilized to make real-time video recordings of the FP-PHP during the experimental process. The Thousand Eyes Wolf high-speed camera has a resolution of 1920×1080, a frame rate of 2000 fps. The pressure sensor used in the experiment is an absolute pressure sensor manufactured by Shanghai Yatan Instrumentation Co. Its model number is STG03-3Bar(A)-1-1-1-2-00-1-0. This pressure sensor has a measurement range of 0 to 3 bar absolute pressure and an accuracy of 0.3%. The maximum continuous operating temperature for the sensor is 120 ℃, and it produces an output signal of 4-20 mA. The pressure sensor is attached using a threaded connection.
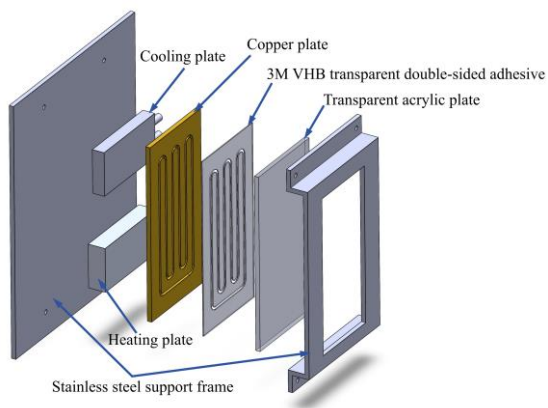
Fig.2 FP-PHP test body split view
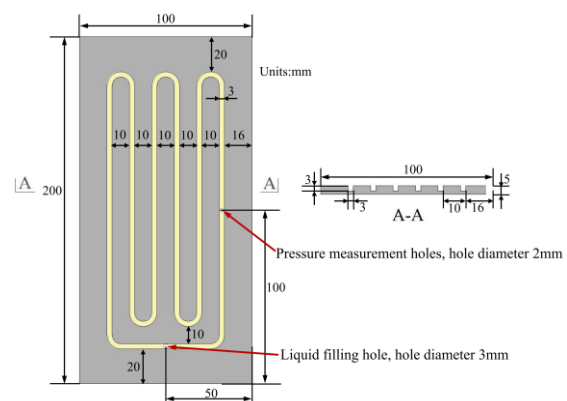
Fig.3 Copper plate size design drawing

The dimensional design of the copper plate is illustrated in Fig. 3. The material of the plate is brass, and its overall dimensions are 100 mm × 200 mm × 5 mm (length × width × height). The condensing section of the FP-PHP measures 40 mm in length, the adiabatic section is 70 mm long, and the evaporating section measures 50 mm. A rectangular channel with cross-sectional dimensions of 3 mm × 3 mm is cut into one side of the copper plate. Additionally, a channel with the same shape as that in the copper plate is processed on 3M VHB transparent double-sided adhesive, measuring 3 mm × 1 mm. Consequently, the cross-sectional dimensions of the FP-PHP in this experiment are 3 mm × 4 mm, giving it a hydrodynamic diameter of 3.4 mm. A total of 10 thermocouples were installed, with 8 positioned on the backside of the copper plate, as shown in Fig. 4. Thermocouples T_1 and T_2 were placed in the evaporation section, T_3 to T_5 were located in the adiabatic section, and T_6 to T_8 were situated in the condensation region. Additionally, T_9 and T_{10} were installed at specific locations on the inlet and outlet pipes of the cooling plate, respectively. FP-PHP utilize deionized water as the working fluid. The liquid filling rate for the FP-PHP is set at 60%. The liquid filling rate is determined by measuring the weight difference of the FP-PHP before and after filling with liquid. The liquid-filled tube, which has an inner diameter of 1 mm and a wall thickness of 1 mm, was soldered to the back of the FP-PHP using solder wire. Prior to filling the heat pipe with deionized water, a rotary vane vacuum pump was employed to evacuate the FP-PHP to a pressure of 2 Pa. Once the liquid filling was completed, sealing pliers were used to clamp the liquid-filled tube, ensuring it was properly sealed. The experimental heating power was varied from 0 to 140 W, with increments of either 10 W or 20 W. The inclination angle of the pulsating hot plate was adjusted using a rotatable platform, with the angle defined as the position between the copper plate and the horizontal plane, as illustrated in Fig. 5. All experiments were conducted at a room temperature of 20 ± 2 ℃.
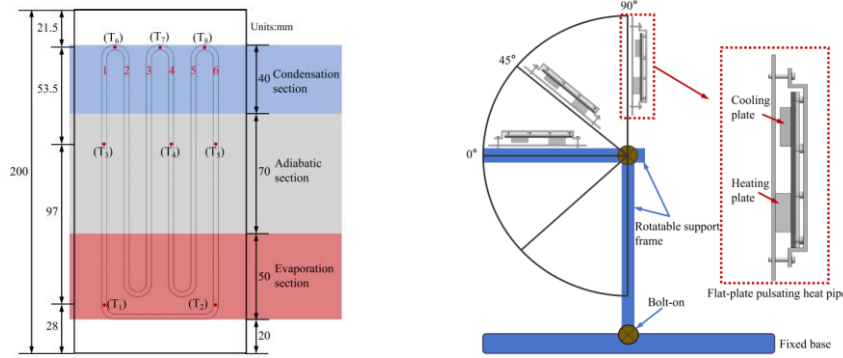
Fig.4 Thermocouple layout points   Fig.5 Schematic diagram of inclination angle change

2.2. Experimental Data Processing

The average temperatures of the evaporation section (T_e), and the condensation section (T_c) of the FP-PHP are calculated using the measured temperature data. The equations are as follows:

$$T_e = \frac{T_1 + T_2}{2}, T_c = \frac{T_6 + T_7 + T_8}{3} \tag{1}$$

The temperature difference ($\varDelta T$) between the hot and cold ends of the FP-PHP, as well as the heat transfer thermal resistance (R), are calculated as follows:

$$\Delta T = T_e - T_c \tag{2}$$

$$R = \frac{\Delta T}{Q_{in}} \tag{3}$$

4

Where Q_{in} represents the heat transfer of the FP-PHP, W. It is important to note that during the heat transfer process, there is an unavoidable heat loss in the FP-PHP, which causes the heat transfer to the cooling water (Q_c) to be lower than the heating power (Q). Consequently, this paper adopts the average of the heating power and the cooling water heat transfer as the effective heat transfer for the FP-PHP in the experimental process. This methodology has been utilized by many researchers when calculating heat transfer [12–14]. The specific equations used for these calculations are as follows:

$$Q_c = c_p q_m (T_{10} - T_9) \tag{4}$$

$$Q = UI \tag{5}$$

$$Q_{in} = \frac{Q_c + Q}{2} \tag{6}$$

Where Q_c is the heat transfer of cooling water, W, c_p is the constant pressure specific heat capacity of cooling water, J/(kg·℃), and q_m is the mass flow rate of cooling water, kg/s. Q is the heating power, W, U is the input voltage, V, and I is the input current, A. The measurement errors in this experiment primarily stem from factors such as temperature, cooling water flow, input voltage, and input current. To monitor temperature, we employed K-type thermocouples, which have an accuracy of up to 0.1 ℃. The minimum temperature difference recorded between the inlet and outlet water of the cooling plate was 1.6 ℃, and the rotameter's measurement accuracy is ± 2.5%. Using this data, we calculated the uncertainty of Q_c to be 8.8% according to Eq. (8). The accuracy of the input voltage (U) of the heating plate is 0.1 V, while the accuracy of the input current (I) is 0.01 A. The minimum set voltage in the experiment is 30 V, and the minimum current is 0.33 A. Consequently, the uncertainty of the heating power (Q) is calculated from Eq. (7) as 3.0%. Additionally, the minimum temperature difference between the hot and cold ends of the FP-PHP was 14.3 ℃. Therefore, the uncertainty of the thermal resistance of the FP-PHP is calculated from Eq. (9) as 9.3%.

$$\frac{\delta(Q)}{Q} = \sqrt{\left(\frac{\delta(U)}{U}\right)^2 + \left(\frac{\delta(I)}{I}\right)^2} \tag{7}$$

$$\frac{\partial Q_c}{Q_c} = \sqrt{(\frac{\partial q_m}{q_m})^2 + \frac{\partial(T_9)^2 + \partial(T_{10})^2}{(T_{10} - T_9)^2}} \tag{8}$$

$$\frac{\partial R}{R} = \sqrt{(\frac{\partial Q_c}{Q_c})^2 + (\frac{\partial Q}{Q})^2 + \frac{\partial T_e^2 + \partial T_c^2}{(T_e + T_c)^2}} \tag{9}$$

3. Experimental results and analysis

3.1. Vapor-liquid distribution of a FP-PHP after initial filling and at the end of oscillation

Fig. 6 and 7 illustrate the vapor-liquid distribution within the FP-PHP both after initial filling and at the end of oscillation, respectively. The position of the liquid filling port influences the flow of liquid inside the FP-PHP. During the filling process, the liquid continuously moves along both sides of the pipe toward the center. This flow results in an unpredictable distribution of liquid after initial filling, exhibiting a degree of randomness. However, numerous experimental observations indicate that, at the beginning, bubbles within the tube form clusters in the liquid. These bubble clusters remain stable in a room temperature environment, as shown in Fig. 6(a). This finding somewhat differs from the research conducted by previous researchers [15]. When the FP-PHP completes the oscillatory motion under the action of heating power and cools down to room temperature, the vapor-liquid

distribution state of the working fluid matter inside the pipe is changed. At this time, the liquid is mainly concentrated in the lower side of each pipe, and the gas is located in the upper side of the pipe. The volume occupied by the liquid in each channel is also not regular and is not affected by the initial vapor-liquid distribution, as shown in Fig. 7(a).

After the oscillation of the FP-PHP concludes, no bubble clusters are observed in the tube. This can be analyzed in relation to the mechanism behind bubble cluster generation. At the completion of the initial liquid filling, the reason for the formation of bubble clusters is that the pressure inside the tube is very low before the liquid is introduced, resulting in a low corresponding saturation temperature. As a result, the working liquid evaporates immediately upon being filled into the tube. In the absence of external forces, the bubble clusters are maintained by surface tension. During the experiment, the working fluid inside the tube undergoes a complex process of evaporation and condensation, leading to the disappearance of the bubble clusters. By the end of the experiment, the pressure inside the tube fluctuates around the saturation vapor pressure corresponding to room temperature. The tube is no longer in the extremely low-pressure environment that existed prior to liquid filling, which means the conditions for bubble clusters no longer exist. It is also important to note that in this experiment, the vapor-liquid distribution state of the FP-PHP, at both the beginning and the end, is unaffected by the inclination angle and heating power; all working conditions adhere to this behavior.

(a) **(b)**
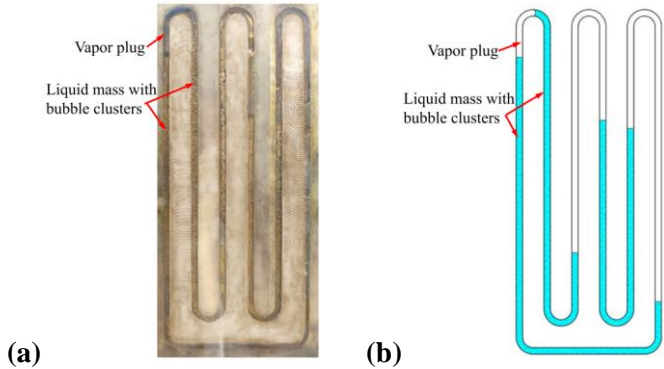
Fig.6 Vapor/liquid plug distribution after initial filling of a FP-PHP: (a) Physical drawing; (b) Schematic diagram

(a) **(b)**
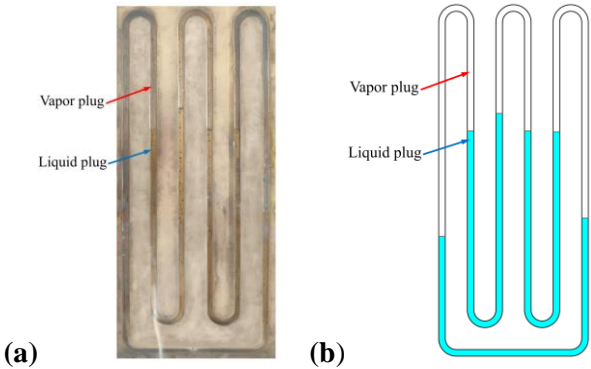
Fig.7 Vapor/liquid plug redistribution at the end of FP-PHP oscillation: (a) Physical drawing; (b) Schematic diagram

Fig. 8 presents visualization images of the start-up for pipe 2 and pipe 3 at an inclination angle of 90° and a heating power of 20 W. The images captured during the start-up process, shown in Figure 8,

reveal key observations. From the period between t + 37 seconds and t + 157 seconds, it is evident that as the evaporation section of the FP-PHP is heated, the initial bubble clusters within the pipe absorb heat and begin to expand. These bubbles merge with one another, ultimately transforming into vapor plugs that move towards the condensation section. After the bubble clusters disappeared, nucleated bubbles began to form in the evaporation section of the FP-PHP between t + 149s and t + 163s. It is important to note that, due to the low heating power during this period, both the rate of bubble growth and rupture were minimal. Consequently, the frequency and amplitude of the oscillations of the working fluid were also low. As a result, a white haze, along with small water droplets adhering to the walls, could be seen in the gas column located at the upper part of the long liquid column. The reason for this phenomenon may be that when a liquid is heated, not only are nucleated bubbles generated, but there is also evaporation occurring at the liquid's surface. This evaporation increases the relative humidity of the surrounding gas. As the humid gas moves toward a condensing section with lower wall temperatures, the liquid present in the gas precipitates and condenses, ultimately forming small droplets that adhere to the wall.
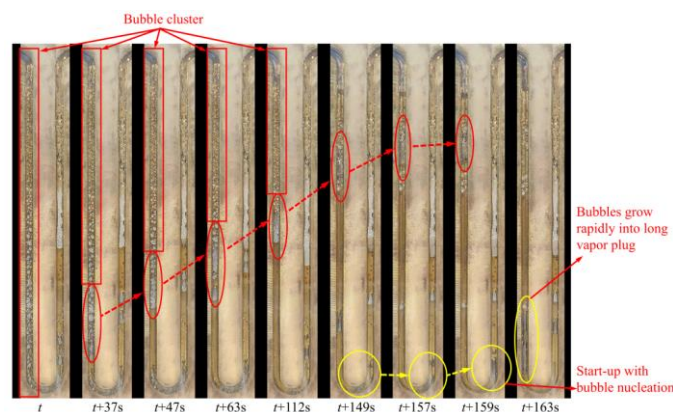
Fig.8 Changes in flow pattern during the start-up phase of a FP-PHP

3.2. Effect of heating power on the start-up and heat transfer characteristics of FP-PHP

Fig. 9 illustrates the temperature variation at each measurement point of the FP-PHP with a 90° inclination under different heating power conditions. The data indicates that the temperature curves generally exhibit a linear upward trend during the start-up phase. When the heating power is set to 40 W, the start-up time and the time required to reach quasi-steady state operation of the FP-PHP are notably longer than those for power levels of 80-120 W. Specifically, the start-up time for the FP-PHP at 40 W is 486 seconds, and it achieves the quasi-steady state operation stage at 985 seconds, following an extended transition period. In contrast, for a heating power of 80 W, the start-up time is reduced to 263 seconds, with the quasi-steady state being reached at 612 seconds. This highlights that increasing the heating power significantly shortens both the start-up time and the time required to achieve a quasi-steady state operation.

The analysis of Fig. 9 reveals that as the heating power increases, the wall temperature curve of the FP-PHP exhibits a rising oscillation frequency and a decreasing oscillation amplitude after reaching the quasi-steady state operation stage. This behavior indicates that the oscillation frequency of the working fluid within the tube increases, the stagnation time decreases, and the overall heat transfer performance improves. However, when the heating power is increased to 120 W, the FP-PHP demonstrates a low-frequency, high-amplitude oscillation characteristic after initially experiencing

high-frequency, low-amplitude oscillations, as illustrated in Fig. 9(d). To analyze the reasons behind this phenomenon, this paper examines the distribution of the primary flow patterns within the FP-PHP during the quasi-steady state operation stage, focusing on the 300 seconds leading up to the end of each condition, as shown in Fig. 10. From Fig. 10(a), it is evident that at a heating power of 40 W, the evaporation section is predominantly characterized by long vapor plugs. The annular flow that forms is quickly transformed into these vapor plugs. The oscillation frequency and amplitude of the working fluid in the tube between the hot and cold ends are low. In Fig. 10(b) and 10(c), when the heating power is increased to 80 W and 100 W, clear annular flow appears in some of the elbows of the evaporation section. Additionally, both upward and downward flows can be observed between adjacent pipes. In the rising flow pipe, the evaporation section is primarily dominated by gas, while in the falling flow pipe, the section is dominated by liquid and bubble flow. At this stage, the working fluid in the hot and cold ends of the FP-PHP exhibits high-frequency and high-amplitude oscillatory movement, resulting in improved heat transfer performance. When the heating power is increased further to 120 W, the falling flow pipe gradually transforms into a rising flow pipe. At this stage, the gas phase is primarily concentrated in the evaporation section, while the liquid phase is mostly found in the adiabatic section and the condensation section. The unbalanced pressure difference between the pipelines is reduced, which decreases the frequency and amplitude of fluid oscillation between the hot and cold ends of the FP-PHP. Notably, at this point, no significant dry-out phenomenon is observed in the annular flow of the evaporation section. Therefore, the observed decrease in the oscillation frequency of the temperature curve can be attributed to a reduction in the frequency of large oscillations of working fluid between the hot and cold ends of the FP-PHP. The current heat transfer limit of the FP-PHP is 120 W. In the following section, we will further analyze the heat transfer characteristics of the FP-PHP under a heating power condition of 140 W.
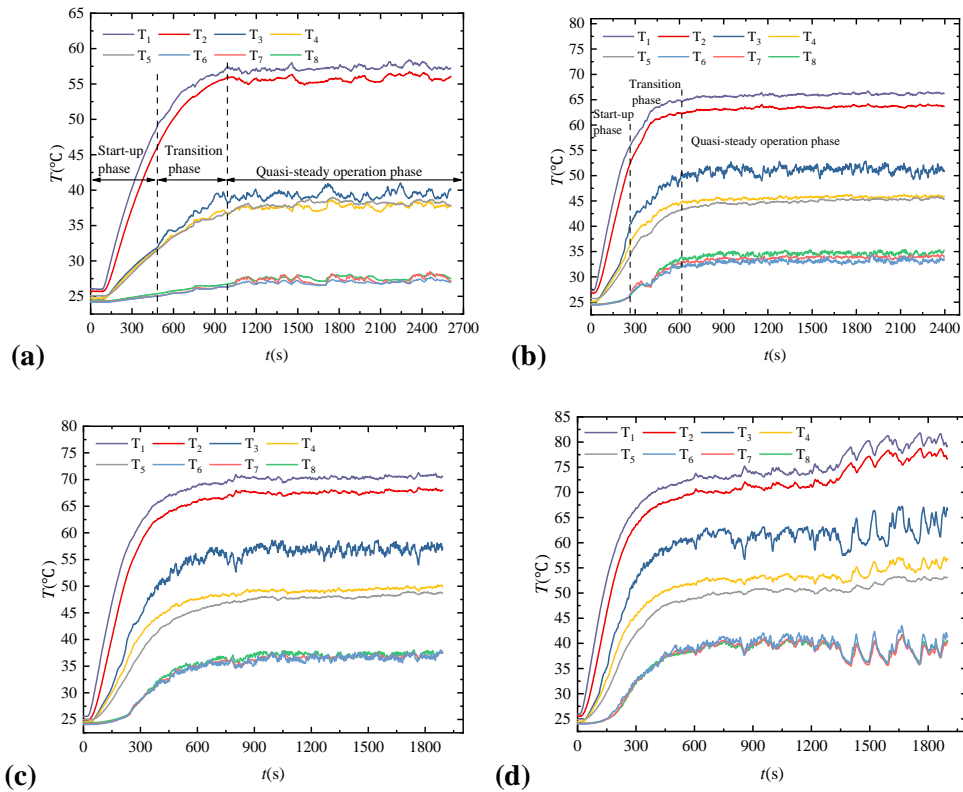
Fig.9 Wall temperature at different heating powers: (a) 40W; (b) 80W; (c) 100W; (d) 120W
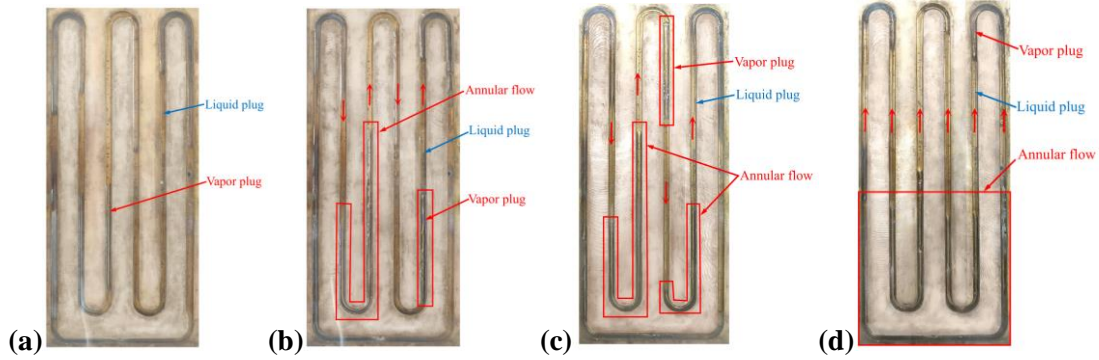
Fig.10 Visualization pictures at different heating powers: (a) 40W; (b) 80W; (c) 100W; (d) 120W

3.3. Effect of inclination angle on the start-up and heat transfer characteristics of a FP-PHP

The variation of wall temperature with heating power for FP-PHP with 60% liquid filling rate at different inclination angles is given in Fig. 11. From the figure, it can be seen that the FP-PHP at 90°, 45° and 0° inclination angle starts to oscillate at 20 W, 30 W and 30 W, respectively. Under the current experimental conditions, the FP-PHP at a 0° inclination can still function normally, albeit with lower oscillation frequency and amplitude of the working fluid inside the pipe. When the heating power is set at 100W, the temperatures (T_1) observed in the evaporation section of the FP-PHP are 63.7 ℃ for the 90° angle, 72.9 ℃ for the 45° angle, and 92.7 ℃ for the 0° angle. This indicates that the inclination angle significantly affects both the start-up behavior and the heat transfer efficiency of the FP-PHP. Notably, the 90° inclination angle allows the evaporating section's wall temperature to remain lower, suggesting that the FP-PHP at a 90° angle exhibits superior start-up and heat transfer performance. It is important to note that, as shown in Fig. 11(a), when the heating power reaches 140 W, there is a sudden and sharp increase in the temperature of both the evaporating section and the adiabatic section of the FP-PHP. In contrast, the temperature of the condensing section begins to decline. This behavior results in an increased temperature difference between the hot and cold ends of the FP-PHP, contributing to a deterioration in heat transfer performance. To better understand the reasons for this heat transfer deterioration, this paper will further analyze the changes in pressure and fluid flow patterns of the FP-PHP under conditions of 90° inclination and 140 W heating power.

(a) 90°   **(b) 45°**   **(c) 0°**
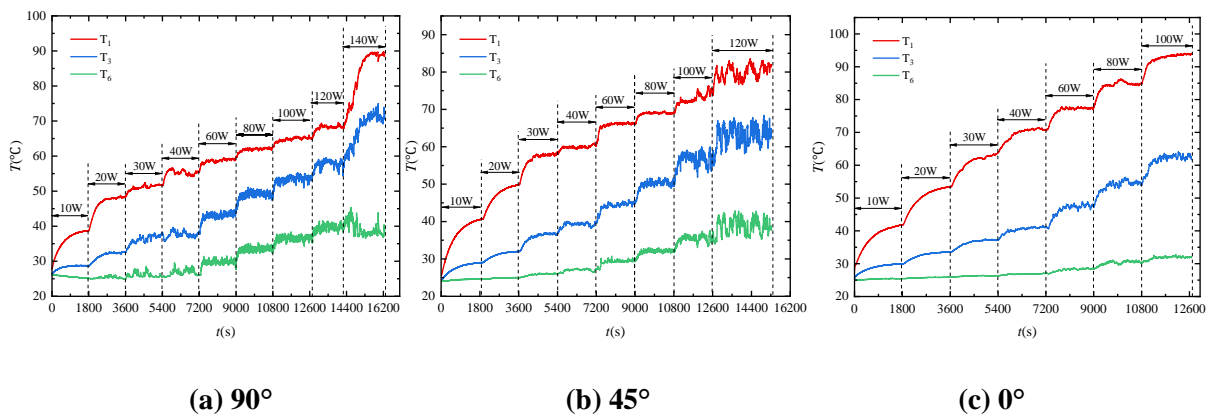
Fig.11 Variation of wall temperature with heating power for FP-PHP at different inclinations

Fig. 12 illustrates how the pressure inside the tube of the FP-PHP varies with heating power at a 90° inclination. The data shows that as the heating power increases, the pressure within the tube also

rises. Notably, when the FP-PHP begins to oscillate at a heating power of 20 W, the pressure curve starts to exhibit clear oscillation features. At 140 W, there is a significant increase in pressure within the tube, and this is accompanied by a similar change in the temperature curve. Fig. 13 illustrates the distribution of the primary flow patterns in the FP-PHP during steady-state operation at a heating power of 140 W. When compared to the heating power of 120 W (as shown in Fig. 10(d)), the volume of annular flow in the evaporation section of the FP-PHP at 140 W is increased. All pipes are oriented for upward flow, and a noticeable localized drying phenomenon can be observed in the evaporation section. Additionally, the flow pattern distribution among the pipes is highly similar, resulting in a reduced imbalance in the pressure difference across the pipes, which complicates working fluid circulation within them. The reflux of the liquid in the condensing section is hindered, leading to an increase in the superheat of the gas in the evaporation section. This rise in superheat causes an increase in the pressure within the tube. As the pressure increases, the saturation temperature of the liquid phase also rises, which negatively impacts the phase change heat transfer of the liquid. Consequently, the heat transfer performance of the FP-PHP deteriorates under high heating power conditions.
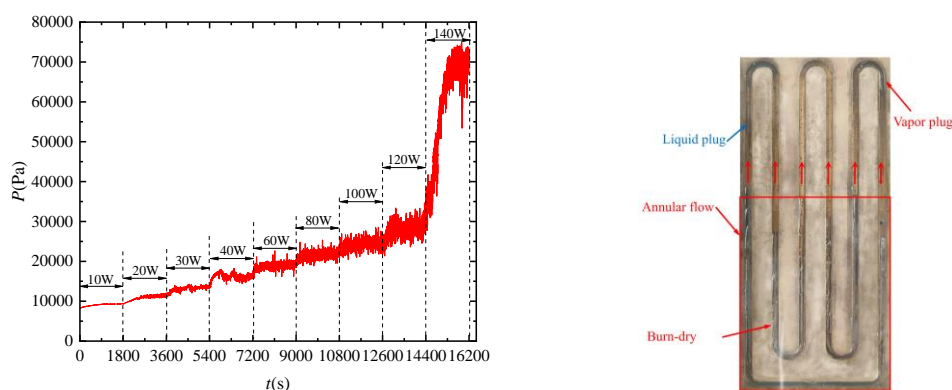
Fig.12 Pressure progression with time   Fig.13 Visualization picture at 140W heating power

The variation in thermal resistance of a FP-PHP with heating power at different inclination angles is shown in Fig. 14. From the figure, it is evident that the thermal resistance is lowest when the inclination angle is 90°. Additionally, the thermal resistance at a 45° inclination angle is lower than that at a 0° inclination angle. From the figure, it can also be observed that the increase in heating power does not offset the effect of the inclination angle on the heat transfer performance of the pulsating heat pipe, because the change in inclination angle affects the magnitude of the gravitational force that promotes the return of the liquid into the evaporation section, and the magnitude of the buoyancy force that promotes the movement of the gas into the condensation section, which will have an effect on the frequency and amplitude of the oscillations of the working fluid in the tube.
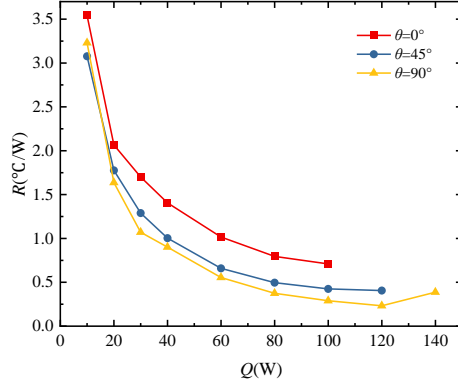
Fig.14 Thermal resistance dependance on heating power

4. Conclusion

In this paper, we present a visual experimental study of a FP-PHP with a rectangular cross-section and a liquid filling rate of 60%. We systematically investigated the start-up and heat transfer performance of the FP-PHP under various inclination angles and heating powers through experimentation. The main conclusions drawn from the study are as follows:

(1) After initially filling the FP-PHP, the distribution of liquid phase within the tube is unpredictable and somewhat random. However, based on numerous experimental observations, it can be established that the initial bubbles within the tube appear as bubble clusters in the liquid phase. The vapor-liquid distribution state of the FP-PHP, after the initial liquid filling and at the conclusion of the experiment, remains unaffected by the inclination angle or heating power, and this behavior consistently applies across all working conditions.

(2) As heating power increases, the start-up time and the time taken to reach a quasi-steady state operation in the FP-PHP are significantly reduced. Under the current experimental conditions, a distinct nucleation start-up process can be observed in the evaporation section of the FP-PHP. The heat transfer limit of the FP-PHP is 120 W.

(3) In this experiment, the FP-PHP with a 90° inclination angle demonstrated superior start-up and heat transfer performance. The inclination angle significantly influences the gravitational force that encourages the liquid to flow back into the evaporation section, as well as the buoyancy force that assists the gas in moving toward the condensation section. While the FP-PHP can still start normally at a 0° angle, the frequency and amplitude of the oscillation of the working fluid in the tube are lower at this position, resulting in poorer heat transfer performance.

(4) When the heating power ranges from 0 to 120 W, the thermal resistance of the FP-PHP decreases as the heating power increases, indicating improved heat transfer performance. The FP-PHP at a 90° inclination angle exhibits the lowest thermal resistance. However, when the heating power is increased to 140 W, there is a sudden rise in both wall temperature and pressure inside the FP-PHP. In this case, the thermal resistance escalates from 0.51 °C/W at 120 W to 0.75 °C/W, which is associated with the burn-dry phenomenon occurring in the evaporation section of the annular flow.

Nomenclature

T	– Temperature, [℃]	T_e	– Average temperature of the evaporation section, [℃]
Q_{in}	– FP-PHP heat transfer, [W]	T_c	– Average temperature of the condensing section, [℃]
Q	– Heating power, [W]	ΔT	– Temperature difference between hot and cold ends, [℃]
R	– Thermal resistance, [℃/W]	Q_c	– Cooling water heat transfer, [W]
U	– Voltage, [V]	q_m	– Cooling water flow rate, [kg/s]
I	– Current, [A]	c_p	– Constant pressure-specific heat capacity, [J/kg·℃]
P	– Pressure, [Pa]	t	– Time, [s]

References

[1] Maydanik, Y. F., et al., Compact Cooler For Electronics On The Basis Of A Pulsating Heat Pipe, Appl. Therm. Eng., 29 (2009), 17-18, pp. 3511-3517

[2] Qu, J., et al., Experimental Investigation Of Silicon-Based Micro-Pulsating Heat Pipe For Cooling Electronics, Nanoscale Microscale Thermophys. Eng., 16 (2012), 1, pp. 37-49

[3] Lin, Z., et al., Heat Transfer Characteristics And LED Heat Sink Application Of Aluminum Plate Oscillating Heat Pipes, Applied Thermal Engineering, 31 (2011), 14-15, pp. 2221-2229

[4] Markal, B., Varol, R., Thermal Investigation And Flow Pattern Analysis Of A Closed-Loop Pulsating Heat Pipe With Binary Mixtures, Journal of the Brazilian Society of Mechanical Sciences and Engineering, 42 (2020), 10, pp. 549

[5] Czajkowski, C., et al., Experimental Study On A Large Scale Pulsating Heat Pipe Operating At High Heat Loads, Different Adiabatic Lengths And Various Filling Ratios Of Acetone, Ethanol, And Water, Appl. Therm. Eng., 165 (2020), pp. 114534

[6] Tseng, C. Y., et al., Investigation Of The Performance Of Pulsating Heat Pipe Subject To Uniform/Alternating Tube Diameters, Exp. Therm. Fluid Sci., 54 (2014), pp. 85-92

[7] Srikrishna, P., et al., Experimental Investigation Of Flat Plate Closed Loop Pulsating Heat Pipe, Heat Mass Transfer, 55 (2019), 9, pp. 2637-2649

[8] Ji, Y., et al., An Experimental Investigation On The Heat Transfer Performance Of A Liquid Metal High-Temperature Oscillating Heat Pipe, International Journal of Heat and Mass Transfer, 149 (2020), pp. 119198

[9] Han, X., Review Of The Development Of Pulsating Heat Pipe For Heat Dissipation, Renewable and Sustainable Energy Reviews, (2016)

[10] Tong, B. Y., et al., Closed-Loop Pulsating Heat Pipe, Applied Thermal Engineering, (2001)

[11] Liu, X., et al., Dynamic Performance Analysis On Start-Up Of Closed-Loop Pulsating Heat Pipes (CLPHPs), Int. J. Therm. Sci., 65 (2013), pp. 224-233

[12] Yang, K. S., et al., Micro Pulsating Heat Pipes With Alternate Microchannel Widths, Appl. Therm. Eng., 83 (2015), pp. 131-138

[13] Chien, K. H., et al., A Novel Design Of Pulsating Heat Pipe With Fewer Turns Applicable To All Orientations, Int. J. Heat Mass Transfer, 55 (2012), 21-22, pp. 5722-5728

[14] Spinato, G., et al., Operational Regimes In A Closed Loop Pulsating Heat Pipe, Int. J. Therm. Sci., 102 (2016), pp. 78-88

[15] Khandekar, S., et al., Multiple Quasi-Steady States In A Closed Loop Pulsating Heat Pipe, Int. J. Therm. Sci., 48 (2009), 3, pp. 535-546